

## Article

# Water Influence on the Determination of the Rock Matrix Bulk Modulus in Reservoir Engineering and Rock-Fluid Coupling Projects

Dariusz Knez <sup>\*</sup>, Mitra Khalilidermani <sup>\*</sup> and Mohammad Ahmad Mahmoudi Zamani 

Department of Drilling and Geoengineering, Faculty of Drilling, Oil and Gas, AGH University of Science and Technology, 30-059 Krakow, Poland

<sup>\*</sup> Correspondence: knez@agh.edu.pl (D.K.); mitra@agh.edu.pl (M.K.); Tel./Fax: +48-12-617-3784 (D.K.)

**Abstract:** This research was conducted to determine how the incorporation of different poroelastic equations would affect the measured rock matrix bulk modulus in the laboratory. To do this, three experimental methods were used to measure the matrix bulk modulus,  $K_s$ , of seven sandstone specimens taken from the Świętokrzyskie mine in Poland. Those experimental methods were based on the different governing equations in poroelasticity theory. The matrix bulk modulus has a substantial impact on the rock strength against external stresses. Moreover, the rock bulk modulus depends directly on two components: the pore fluid bulk modulus and matrix bulk modulus. The second one is more important as it is much higher than the first one. In this study, the accuracy of those three methods in the measurement of the matrix bulk modulus was evaluated. For this purpose, an acoustic wave propagation apparatus was used to perform the required tests. For each method, an empirical correlation was extracted between the matrix bulk modulus and the applied hydrostatic stress. In all the experiments, an exponential correlation was observed between the matrix bulk modulus and the hydrostatic stress applied on the rock. Furthermore, it was found that the incorporation of the dry bulk modulus in the calculations led to an underestimation of the matrix bulk modulus. In addition, as the hydrostatic stress was raised, the matrix bulk modulus also increased. The applied methodology can be deployed to determine the matrix bulk modulus in coupled rock-fluid problems such as reservoir depletion, hydraulic fracturing, oil recovery enhancement, underground gas storage and land subsidence.

**Keywords:** pore pressure; carbon sequestration; fluid injection; poroelasticity; compressibility; reservoir engineering; unconventional reservoir; Skempton's coefficient; Biot's coefficient; improved oil recovery



**Citation:** Knez, D.; Khalilidermani, M.; Zamani, M.A.M. Water Influence on the Determination of the Rock Matrix Bulk Modulus in Reservoir Engineering and Rock-Fluid Coupling Projects. *Energies* **2023**, *16*, 1769. <https://doi.org/10.3390/en16041769>

Academic Editors: Mofazzal Hossain and Zacariah Hildenbrand

Received: 18 October 2022

Revised: 16 January 2023

Accepted: 8 February 2023

Published: 10 February 2023



**Copyright:** © 2023 by the authors. Licensee MDPI, Basel, Switzerland. This article is an open access article distributed under the terms and conditions of the Creative Commons Attribution (CC BY) license (<https://creativecommons.org/licenses/by/4.0/>).

## 1. Introduction

Common geoengineering projects deal with diverse soil and rock layers. In those layers, the pore fluid acts as a prohibitive or, reversely, a contributing factor during the execution phase of the projects. For instance, in petroleum engineering, the pore pressure within the hydrocarbon-bearing formation is critically influential for the acquisition of higher production rates. However, hydrocarbon extraction gradually leads to the dissipation in the pore pressure in the reservoir and a reduction in the production rate. In this case, different enhanced oil recovery (EOR) techniques are utilized to increase the production rate. For this purpose, usually water or carbon dioxide (CO<sub>2</sub>) is injected through the depleted reservoir, thereby increasing the pore pressure in the rocks. Another similar case is the CO<sub>2</sub> injection to the depleted reservoirs in carbon sequestration projects. In both examples, the interaction between the pore fluid and rock solid (skeleton) creates mutual stress and deformations in the rock mass layer. In this situation, such induced stress moves the pore fluid within the rocks, thereby leading to a successful implementation of the EOR or the carbon sequestration operation [1].

In nature, porous rocks contain different fluid types, mainly water. The near-surface porous rocks are subjected to the stresses originated from the overburden pressure [2]. Such overburden pressure is derived from the weight of the overlying rock layers.

Under such loading conditions, the rock is continuously under compression, tension, or shear stresses. Hence, the rock volume changes when the surrounding stress increases and decreases. The magnitude of such volumetric deformation directly depends on the rock bulk modulus. In the poroelasticity theory, based on the loading conditions, several bulk moduli have been defined for rocks, e.g., the undrained bulk modulus, drained bulk modulus, dry bulk modulus and matrix bulk modulus. In this research, the measurement of the latter case is the main objective. In what follows, the relevant literature is presented.

In a small element of a porous rock, the overburden pressure is borne by the fluid pressure and the solid matrix (skeleton) [3]. The resistance of the matrix against the applied external stresses is described through the concept of the matrix compressibility. In the literature, other definitions such as the skeleton compressibility, mineral compressibility and solid compressibility have also been used by different researchers. In this work, the term “matrix” is uniformly used to refer to the solid skeleton of the rocks. The matrix compressibility depicts the tendency of the rock grains to compact (compression). When the matrix compressibility is higher, the resistance of the grains against the compaction is lower.

Generally, the concept of compressibility is an integral part in the poroelasticity theory. The poroelasticity theory was established by Maurice Anthony Biot [4], who completed the Terzaghi’s effective stress law [3] by introducing the Biot’s coefficient. There are several types of compressibility defined in this theory, including the rock bulk compressibility, matrix compressibility and pore compressibility. If a rock is purely composed of one specific mineral, the matrix bulk modulus,  $K_s$ , is equal to that mineral bulk modulus [5,6]. However, in nature, rocks contain various minerals in their structures. As an interesting work, Mavko et al. developed a list of common mineral bulk moduli which can be utilized if no experimental measurement of  $K_s$  is available [7]. The values of  $K_s$  can be measured using static, or dynamic tests. In dynamic tests, the compressional wave velocity ( $V_p$ ) and shear wave velocity ( $V_s$ ) are used to calculate the  $K_s$ . Dynamic tests are more affordable, although the precision of the result is less than static tests.

The matrix-fluid interaction has a considerable effect on the mechanical behavior of the rocks [8,9]. In better words, the pore fluid, e.g., water, can change the elastic moduli, unconfined compression strength (UCS), Poisson’s ratio [10,11], deformability, strength [11,12], the ratio of  $V_p/V_s$  [13], etc. Therefore, the impact of the pore fluid on the mechanical properties of the rocks cannot be ignored. In this study, the UCS test was conducted for both the wet and dry samples to show the sensibility of  $K_s$  to the water presence.

In this study, using the experimental tests in the laboratory, the dynamic matrix bulk modulus of seven sandstone samples taken from the Świętokrzyskie Mine situated in the north of Kielce, Poland, was measured. For this purpose, three different methods were utilized. For each method, an empirical correlation between the matrix bulk modulus and the hydrostatic stress was extracted. The best fitted graphs were found to be exponential curves. In the literature review, a wide range of  $K_s$  values have been reported for the sandstone rocks. Such a range contains  $K_s$  values from 15 GPa to 67 GPa [14].

The structure of the paper has been arranged as follows. Firstly, in Section 2.1, the theoretical concepts relevant to the calculation of the matrix bulk modulus are presented. In this section, the three dynamic methods adopted for the calculation of  $K_s$  are explained. Then, in Section 2 the physical and mechanical properties of the captured sandstone samples are described and then the experimental procedure of the conducted tests are expressed. Afterward, the corresponding results are presented in Section 3 through the tables and figures. Then, in Section 4, the obtained results are profoundly discussed and compared with the previous research. Finally, the paper ends with a concise conclusion describing the key findings, applications and potential recommendations related to future works. The

methods used in this study can be applied for the calculation of  $K_s$  in geoscience engineering applications in which the poroelastic behavior of the rocks is of paramount significance.

## 2. Materials and Methods

### 2.1. Theory of Problem

When a small element of a porous rock is subjected to an external pressure, it resists against the volumetric change. Such resistance stems from the fluid compressibility and the matrix compressibility. The static equilibrium between the pressures (stresses) necessitates that [3]

$$\sigma_v' = \sigma_v - P_p \quad (1)$$

where  $\sigma_v'$  is the effective stress,  $\sigma_v$  represents the total stress and  $P_p$  indicates the pore pressure within the rock element.

If a rock is subjected to an external pressure, the bulk compressibility of the rock is calculated as [2]

$$c_b = -\frac{1}{V_b} \left( \frac{dV_b}{dP} \right)_T \quad (2)$$

where  $c_b$  is the bulk compressibility of the rock,  $V_b$  indicates the initial volume of the rock,  $dV_b$  represents the change in the bulk volume of the rock and  $dP$  is the change in the applied pressure. The subscript  $T$  means that such conditions must be satisfied in the constant temperature. Since the rock volume decreases with the increase in the applied pressure, the negative sign in Equation (2) generates the  $c_b$  as a positive value of the rock.

The matrix compressibility is defined as the fractional change in the volume of the matrix with the change in the applied pressure. It can be stated through the following relationship [2]

$$c_m = -\frac{1}{V_m} \left( \frac{dV_m}{dP} \right)_T \quad (3)$$

where  $c_m$  is the matrix compressibility,  $V_m$  indicates the initial volume of the matrix,  $dV_m$  represents the change in the volume of the matrix and  $dP$  is the change in the applied pressure.

Similarly, the pore compressibility is defined as the fractional change in the volume of the pores with the change in the applied pressure. In petroleum engineering, the pore compressibility is also referred to as the formation compressibility. The pore compressibility can be obtained through the following equation [2]

$$c_p = -\frac{1}{V_p} \left( \frac{dV_p}{dP} \right)_T \quad (4)$$

where  $c_p$  is the pore compressibility,  $V_p$  indicates the initial volume of the pores,  $dV_p$  represents the change in the volume of the pores and  $dP$  is the change in the applied pressure.

The concept of compressibility can be also expressed in the form of the bulk modulus,  $K$ . Indeed, the compressibility is the reciprocal of the bulk modulus. For instance, the matrix compressibility can be expressed as

$$K_s = \frac{1}{c_m} = -V_m \left( \frac{dP}{dV_m} \right)_T \quad (5)$$

where  $K_s$  is the matrix bulk modulus. Based on the above formula,  $K_s$  is directly dependent on the change in the applied pressure,  $dP$ , and the matrix volume change,  $dV_m$ . Therefore, when an external pressure is applied to a porous rock,  $K_s$  is a critical factor in the volumetric change of the matrix (and the rock) [2].

In this research, the aim is to measure the matrix bulk modulus,  $K_s$ , for a set of sandstone samples using an acoustic wave propagation apparatus. To do this, a set of seventeen core samples from a homogenous sandstone rock were taken and prepared for the subsequent laboratory tests. The samples were cylindrical with a consistent diameter of 38 mm. The length of the samples varied in the range of 40–44.5 mm.

Afterward, the rest of the samples were fully saturated with water, and then they were inserted in the acoustic velocity measurement apparatus (AVS). Simultaneously, the compressional and shear acoustic waves were propagated through the rock samples, and the dynamic elastic moduli in both the drained and undrained conditions were calculated. Then, three different methods were applied to calculate the matrix bulk modulus of each sample.

*Method 1:* Having the drained and undrained bulk moduli of each sandstone sample, the corresponding  $K_s$  was calculated as [15]

$$\frac{K_u}{K_s - K_u} = \frac{K}{K_s - K} + \frac{K_f}{\varphi \cdot (K_s - K_f)}. \quad (6)$$

where  $K_u$  and  $K$  represent the undrained and drained bulk modulus, respectively. Moreover,  $\varphi$  represents the rock sample porosity and  $K_f$  is the bulk modulus of the pore fluid. In this research, the pore fluid is water with  $K_f = 2.3$  GPa [16]. Equation (6) shows that the different bulk moduli of a rock depend directly on their porosity. Rock porosity is a key characteristic in the poroelastic behavior of rock samples [17–19].

*Method 2:* In this method, the poroelastic relationship between the Skempton's coefficient and the bulk moduli of the samples was utilized to calculate the matrix bulk modulus of each sample. Skempton's coefficient,  $B$ , is an important poroelastic parameter representing the variation of the pore fluid pressure with the applied hydrostatic stress [9]. This parameter is described as the proportion of the pore pressure change to the hydrostatic stress change under undrained conditions. The corresponding mathematical relationship is expressed as [20]

$$B = \left. \frac{dP_p}{dP_c} \right|_{\Delta m_f = 0}. \quad (7)$$

where  $B$  represents the Skempton's coefficient,  $dP_p$  represents the change in the pore pressure and  $dP_c$  represents the change in the hydrostatic stress. Moreover, the subscript  $\Delta m_f = 0$  means that the mass of the pore fluid remains constant during the conduction of the experiment. In better words, no fluid is injected or released from the sample. In this research, the value of  $B$  was experimentally measured in the laboratory setting.

Furthermore, the Skempton's coefficient can be related to the different rock bulk moduli through the following relationship [20].

$$B = \frac{1 - \frac{K}{K_u}}{1 - \frac{K}{K_s}}. \quad (8)$$

Hence, from the above equation, the value of  $K_s$  can be computed as

$$K_s = \frac{K \cdot B \cdot K_u}{-K_u + K + K_u \cdot B} \quad (9)$$

Equation (9) was utilized to calculate the values of  $K_s$  in the second method. In this study, the hydrostatic stress was raised through constant increments of 3.5 MPa so long as the average Skempton's coefficient remained equal to 1. For the taken sandstone samples, the Skempton's coefficient fluctuated around 1 when the hydrostatic stress was less than 24.5 MPa. Therefore, the applied hydrostatic stress was always held less than 24.5 MPa to avoid potential failure in the sample.

*Method 3:* Similar to the two previous methods, another approach was utilized to compute the values of  $K_s$ . To do this, based on the undrained and drained experiments, the values of Biot's coefficient were first computed for each sample. Biot's coefficient is defined as the ratio of change in the volume of the pore fluid (water) to the change in the bulk volume of the rock sample under the drained condition. Biot's coefficient is mathematically expressed as [21]

$$\alpha = \frac{dV_f}{dV_b} \Big|_{\Delta P_p = 0} \quad (10)$$

where  $\alpha$  represents the Biot's coefficient,  $dV_f$  represents the change in the volume of the pore fluid and  $dV_b$  represents the change in the bulk volume of the sample. Moreover, the subscript  $\Delta P_p = 0$  shows that the measurement must be conducted under a constant pore pressure condition. Commonly, Biot's coefficient varies in the domain of  $\varphi < \alpha \leq 1$ , in which  $\varphi$  indicates the rock porosity [6]. For sandstone specimens,  $\alpha$  is usually between 0.45 and 0.8. In this research,  $\alpha$  was computed through the following equation [21]

$$\alpha = \left( 1 - \left( \frac{K}{K_u} \right) \right) / B. \quad (11)$$

where  $K$  and  $K_u$  indicate the drained and undrained bulk modulus, respectively. Furthermore, Biot's coefficient can be formulated using the dry bulk modulus and the matrix bulk modulus of the rock samples [6,20]

$$\alpha = 1 - (K_{dry}/K_s). \quad (12)$$

where  $K_{dry}$  is the dry bulk modulus. Equation (12) can be rearranged to calculate  $K_s$  as follows.

$$K_s = K_{dry} / (1 - \alpha). \quad (13)$$

The above equation was utilized to calculate the values of  $K_s$  as the third method.

In this research, Equations (6), (9) and (13) were used to calculate the dynamic matrix bulk modulus of the sandstone samples. All the experiments were conducted at room temperature (24 °C). It is noteworthy that the poroelastic parameters are dependent on the temperature because the properties of the pore fluid (water) are sensitive to temperature change [22–24]. The rock-water interaction directly influences the safety and requirements of the engineering projects dealing with the water-bearing porous rocks [25].

In the present research, an acoustic wave propagation (AVS) apparatus was utilized to measure the dynamic bulk modulus of the sandstone samples. Figure 1 shows the applied AVS apparatus. The main units of the AVS apparatus included a core holder, wave receivers, wave transmitters, oscilloscope, a hand pump for applying the hydrostatic stress, pipes of the hydrostatic stress, valves of the hydrostatic stress, pipes of the pore pressure, valves of the pore pressure and relevant monitors for the exhibition of the hydrostatic stress, along with the pore fluid pressure. During the test, the acoustic waves were propagated by the transmitters through the samples, and then the corresponding waves were received by the receivers. Two groups of waves were propagated through each sandstone sample: compressional (P-wave) and shear waves (S-wave). Thus, the velocities of the P-wave and S-wave through the samples were recorded.

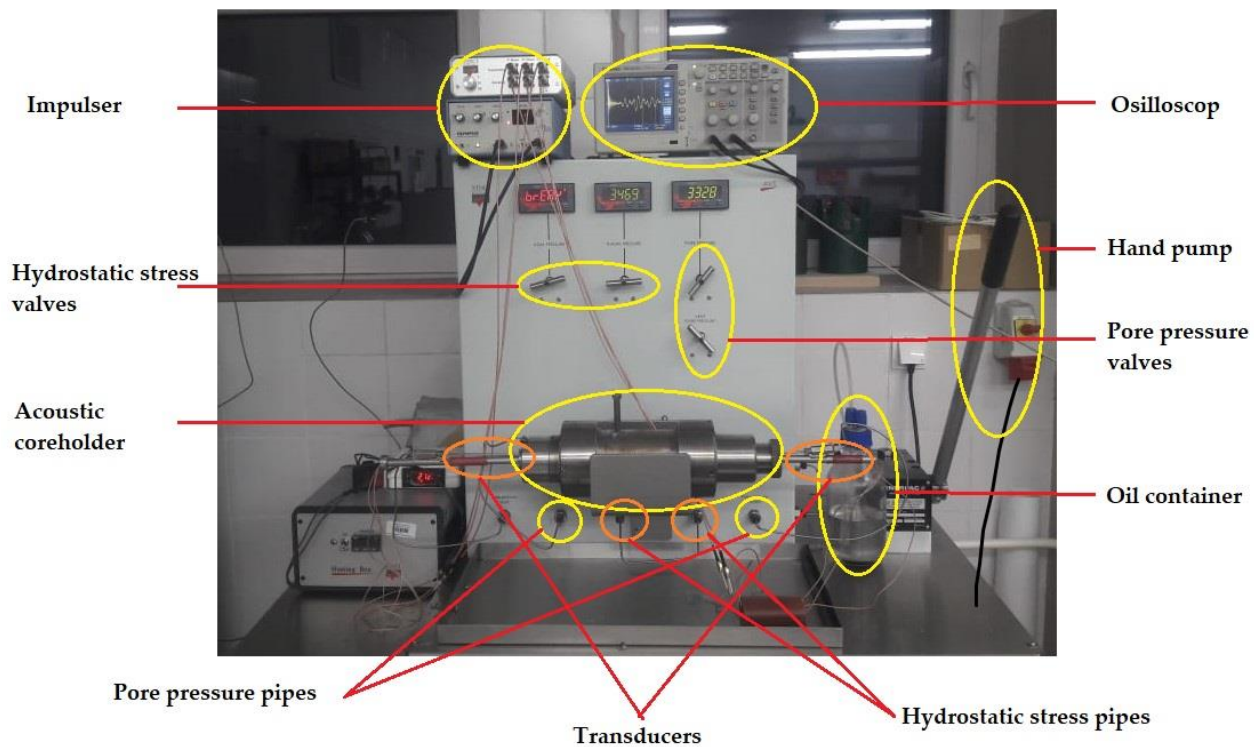


**Figure 1.** Acoustic velocity measurement (AVS) apparatus.

After recording the velocities of the P-wave and S-wave, the dynamic bulk modulus of each sandstone sample was calculated via the following equation [6,15]

$$K_{dyn} = \rho \left( V_p^2 - \frac{4}{3} V_s^2 \right). \quad (14)$$

where  $K_{dyn}$  is the dynamic bulk modulus (Pa). Moreover,  $V_p$  (m/s) and  $V_s$  (m/s) indicate the compressional and shear wave velocities, respectively. Furthermore,  $\rho$  represents the density of the rock ( $\text{kg/m}^3$ ).

In the current study, Equation (14) was used to calculate the dynamic bulk moduli of the sandstone samples in the undrained,  $K_u$ , and drained,  $K$ , conditions.

## 2.2. Materials

In this research, an experimental study was carried out to determine the dynamic matrix bulk modulus of the sandstone samples taken from the Świętokrzyskie Mine located in the north of Kielce, Poland. To capture the necessary core samples, a piece of the sandstone rock was taken from the mine, and then it was transferred to the laboratory. Afterward, using a special cutting machine, seventeen cylindrical samples were taken from the initial piece of rock. The diameter of the samples was 38 mm while the length of the samples varied between 40 to 44.5 mm. Those samples were classified into two groups. Ten samples were selected for UCS measurement. The remaining seven samples were utilized for the acoustic velocity measurement apparatus (AVS) test. Figure 2 demonstrates the appearance of the corresponding sandstone samples. The sandstone grains had pink–white color and were connected suitably via a silica cement. The grain size of the sand particles varied between 0.1–0.2 mm.



**Figure 2.** Appearance of the sandstone samples for the UCS test: dry samples (right), wet samples (middle), for the AVS test (left).

To obtain an initial knowledge about the UCS of the sandstone samples, the first group of samples was subjected to the uniaxial compressive strength apparatus. The corresponding UCS apparatus is shown in Figure 3.



**Figure 3.** The UCS measurement apparatus.

The UCS tests were performed on five wet and five dry samples. The reason was to show the water influence on the weakening of the rock samples. The discrepancy between the obtained UCS values in the dry and wet conditions demonstrated that the mechanical properties of the rock samples were sensitive to the water presence. Tables 1 and 2 illustrate the results pertinent to the UCS measurement. The average UCS of the wet sandstone samples was obtained as 47.8 MPa. On the other side, the average UCS of the dry sandstone specimens was measured as 60.3 MPa. Since the wet samples were used in the AVS apparatus, the average UCS of the wet samples (47.8 MPa) was considered during the AVS tests. In better words, for the conduction of the AVS tests, the hydrostatic stress was always kept less than 47.8 MPa.

**Table 1.** UCS values obtained for the five wet samples.

Sample Code	Diameter (mm)	Length (mm)	UCS (MPa)
UCS1	38	43	43.73
UCS2	38	42	50.33
UCS3	38	43	45.61
UCS4	38	43	51.60
UCS5	38	42	46.02

**Table 2.** UCS values obtained for the five dry samples.

Sample Code	Diameter (mm)	Length (mm)	UCS (MPa)
C1	38	44	60.88
C2	38	41	69.70
C3	38	41	56.30
C4	38	41.5	52.05
C5	38	42	62.44

### 3. Results

After determining the average value of the UCS, the rest of the samples (seven samples) were emplaced in the oven for 24 h to be dried. Then, the samples were taken out from the oven and their dry masses were measured. Afterward, the samples were inserted into a water saturation apparatus for 48 h under the pressure of 14 MPa. To saturate the samples, distilled water was firstly boiled and then it was allowed to reach the room temperature. Afterward, the samples were fully saturated with the boiled distilled water. It is noteworthy that boiling the distilled water removes the air bubbles from the rock pores [7]. Consequently, a complete saturation status (saturation degree = 100%) was ensured. Finally, the water-saturated samples were taken out from the saturation apparatus and their corresponding saturated masses were measured. Having the dry and saturated masses of the samples, their porosity and density were calculated (Table 3). According to the results, the samples had a porosity of approximately around 16%. Furthermore, the average density of the samples was obtained as 2.5 gr/cm<sup>3</sup>.

**Table 3.** Physical properties of the seven sandstone samples.

Sample Code	Diameter (mm)	Length (mm)	Mass <sub>dry</sub> (gr)	Mass <sub>sat</sub> (gr)	Porosity (%)	Density (gr/cm <sup>3</sup> )
Sample 1	38	42.5	99.94	108.21	17.17	2.50
Sample 2	38	44.5	108.30	116.22	15.70	2.55
Sample 3	38	41	98.50	105.63	15.34	2.50
Sample 4	38	41	100.34	107.55	15.51	2.55
Sample 5	38	43	105.29	112.7	15.20	2.55
Sample 6	38	43.5	104.88	112.28	15.01	2.50
Sample 7	38	40	96.24	103.53	16.08	2.53

After determining the physical properties of the sandstone samples, the acoustic wave propagation tests were conducted. To do this, the AVS apparatus (see Figure 1) was used. It was capable of transmitting and receiving the compressional (P-wave) and shear waves (S-wave) in the rock samples. In better words, the rock samples were inserted into the AVS apparatus and the velocities of the P-wave and S-wave in each sample were recorded while the hydrostatic stress was changed in regular increments of 1000 psi (approximately equal to 3.5 MPa).

As already mentioned, for each sample, three types of bulk moduli were directly measured: the undrained, drained and dry bulk moduli. To do this, the experiments for each sandstone sample were carried out under three conditions: undrained, drained and dry conditions.

Regarding the undrained conditions, firstly, each water-saturated sample was emplaced in the core holder. Afterward, the pore pressure pipes were filled with water, and then the corresponding valves were closed to create the undrained conditions. In this case, no water exited from the assembly of the sample and the pipes during the tests (applying the hydrostatic stress to the sample). In the subsequent step, using the hydraulic hand pump, the hydrostatic stress was applied to the sample. It should be mentioned that such hydrostatic stress was applied to the sample through the oil stored in the oil tank. During the test, the hydrostatic stress was regularly raised through a constant increment of 3.5 MPa.

In other words, it was applied as 3.5 MPa, 7 MPa, 10.5 MPa, 14 MPa, 17.5 MPa, 21 MPa and 24.5 MPa.

When the hydrostatic stress was raised, the pore pressure increased within the sample to endure the applied pressure. In fact, the pore pressure withstood the applied hydrostatic stress. Therefore, in each increment, the corresponding Skempton's coefficient was calculated. As previously mentioned in Section 1, the Skempton's coefficient is described as the proportion of the pore pressure change to the hydrostatic stress change when the sample is subjected to a hydrostatic stress under undrained conditions. The hydrostatic stress was raised until the overall Skempton's coefficient remained approximately equal to 1. According to the conducted experiments, the overall Skempton's coefficient remained around 1 when the hydrostatic stress values were less than 24.5 MPa.

In each increment, as well as the hydrostatic stress and pore pressure, the velocities of the P-wave and S-wave were also recorded. Then, Equation (14) was utilized to calculate the dynamic bulk modulus of the sandstone samples in the undrained conditions, i.e.,  $K_u$ . At the end of each undrained test, the values of the direct and indirect Skempton's coefficient was calculated using Equation (7) and Equation (8), respectively. Figure 4 demonstrates the variation of the pore pressure with the hydrostatic stress for the seven sandstone samples.

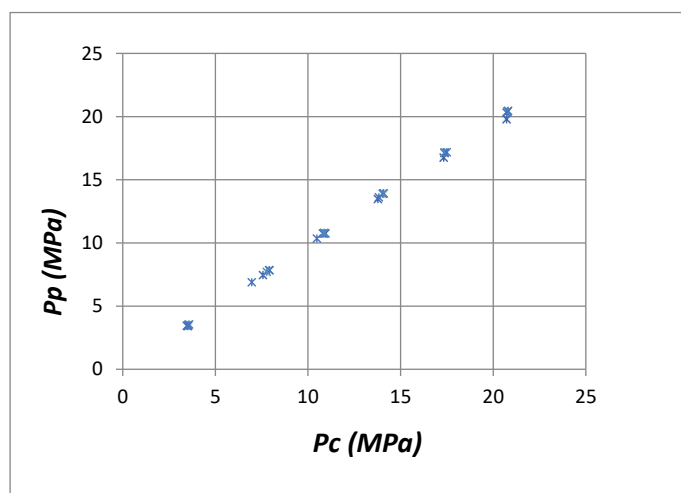


**Figure 4.** Variation of the pore pressure with the hydrostatic stress for the seven samples.

After the conduction of the experiments under the undrained conditions, the hydrostatic stress was released completely. Then, the pore pressure pipes were opened to prepare the apparatus for performing the experiments under the drained conditions. Afterward, the hydrostatic stress was regularly raised in constant increments of 3.5 MPa. In each increment, the values of the hydrostatic stress, P-wave velocity and S-wave velocity were recorded. Note that under the drained conditions, the pore pressure did not change with the hydrostatic stress, and it remained equal to the ambient atmospheric pressure (around 0.1 MPa). Again, Equation (14) was applied to calculate the samples' drained bulk modulus.

After conducting the experiments under the undrained and drained conditions and having the values of  $K_u$  and  $K$  for each sample, the corresponding matrix bulk modulus was calculated for each sample using Equation (6). Figure 5 depicts the variation of the calculated  $K_s$  with the hydrostatic stress. The corresponding empirical correlation between the dynamic matrix bulk modulus and the hydrostatic stress was acquired as

$$K_s = 15.793 P_C^{0.0113} \quad (15)$$

where  $K_s$  represents the matrix bulk modulus (GPa) and  $P_C$  indicates the hydrostatic stress (MPa). Furthermore, the coefficient of determination,  $R^2$ , was obtained at around 0.57, thereby indicating an acceptable agreement between the calculated values of  $K_s$  and the hydrostatic stress. As it can be seen, the dynamic matrix bulk modulus of all the

samples varied from 15.5 GPa to 21.4 with the corresponding values of the hydrostatic stress changing from 3.5 MPa to 24.5 MPa, respectively.

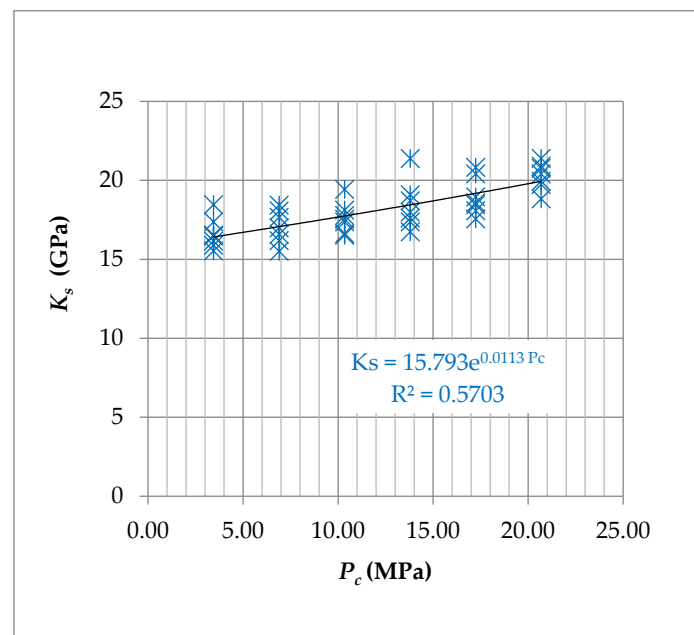


**Figure 5.** Calculated  $K_s$  as a function of the hydrostatic stress (Method 1).

The values of  $K_s$  for all the samples were also calculated using Equation (9) (Method 2). The corresponding results are shown in Figure 6. As it can be seen, the empirical relationship between the  $K_s$  and  $P_c$  was exponential and its trend was similar to the curve extracted for Method 1. The relevant empirical correlation was extracted as

$$K_s = 15.251 P_c^{0.0097} \quad (16)$$

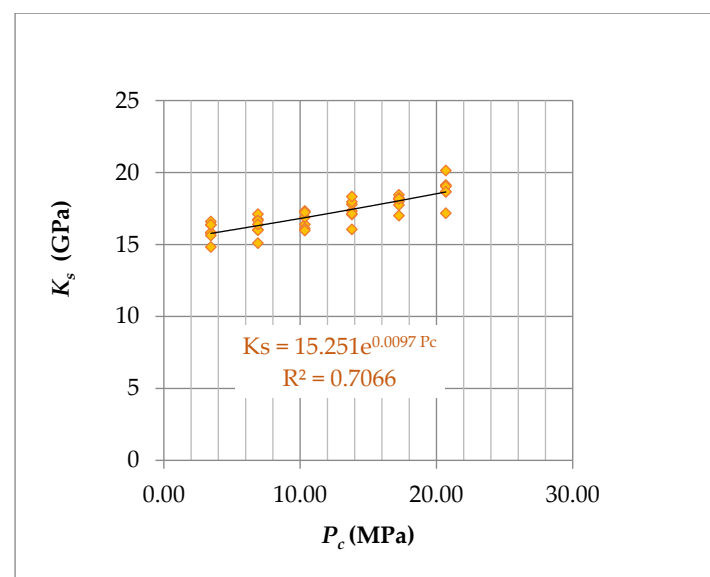


**Figure 6.** Calculated values of  $K_s$  as a function of the hydrostatic stress (Method 2).

In this case, the coefficient of determination,  $R^2$ , was calculated as 0.70, thereby representing a better fitness between the calculated values of  $K_s$  and  $P_c$ . In addition, the minimum and maximum values of  $K_s$  were obtained as 14.8 GPa and 21.1 GPa, respectively.

Generally, the calculated values of  $K_s$  through Method 2 were slightly less than their counterparts obtained in Method 1.

The values of  $K_s$  for all the samples were also calculated using Equation (13) (Method 3). The corresponding graph is shown in Figure 7. As it can be seen, the empirical relationship between  $K_s$  and  $P_c$  was exponential and its trend was similar to the curves obtained via Method 1 and Method 2. The relevant empirical correlation was extracted as

$$K_s = 13.711 P_c^{0.0115} \tag{17}$$

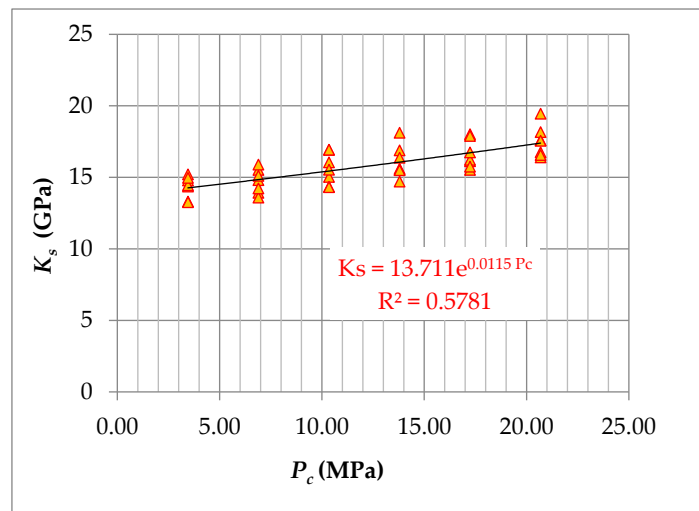


Figure 7. Calculated values of  $K_s$  as a function of the hydrostatic stress (Method 3).

For this case, the coefficient of determination,  $R^2$ , was around 0.57, thereby representing a relatively acceptable fitness between  $K_s$  and  $P_c$ . In addition, the minimum and maximum values of  $K_s$  were obtained as 13.27 GPa and 19.46 GPa, respectively.

The obtained empirical correlations using Method 1, Method 2 and Method 3 are depicted in Figure 8. As it is evident, for a specific value of hydrostatic stress, Method 1, Method 2 and Method 3 delivered the highest, the intermediate and the lowest values of  $K_s$ , respectively.

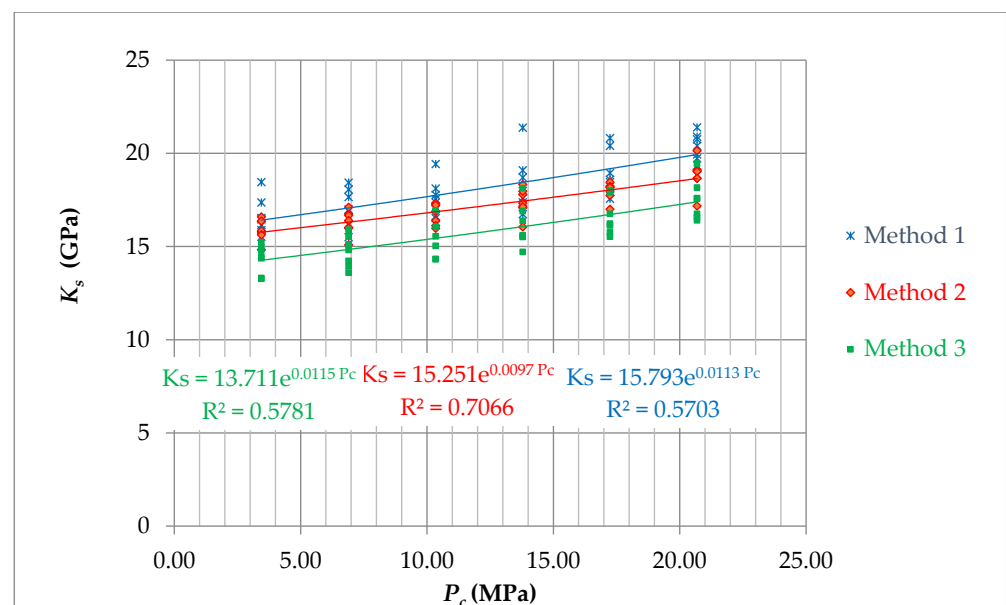


Figure 8. Calculated values of  $K_s$  as a function of the hydrostatic stress for the three methods.

As far as the type of the input parameters is concerned, both dynamic and static parameters were applied to calculate  $K_s$ . In Method 1,  $K$  and  $K_u$  were the dynamic variables and the parameter of  $\varphi$  was directly obtained from the static measurements. The value of  $K_f$  was also assumed to be 2.3 GPa. In Method 2,  $K$  and  $K_u$  were the dynamic parameters while the parameter of  $B$  was directly obtained from the static measurements. In Method 3, the parameters of  $K$ ,  $K_u$  and  $K_{dry}$  were the dynamic parameters. Figure 8 shows that the obtained values using Method 2 were always between the values obtained using Method 1 and Method 3. Furthermore, this method delivered a better fitness between  $K_s$  and the hydrostatic stress. Overall, it seems that Method 1 and Method 3 can be applied for the calculation of the lower and upper bounds of  $K_s$ . Therefore, in this research, the empirical correlation pertinent to Method 2 was deduced to represent the dynamic bulk modulus of the sandstone samples.

#### 4. Discussion

In this research, through the laboratory experiments, the dynamic matrix bulk modulus of seven sandstone samples taken from the Świętokrzyskie mine situated in the north of Kielce, Poland, was determined. To do this, three different methods were applied. For each method, an empirical correlation between  $K_s$  and  $P_c$  was extracted. The best fitted correlations were found to be exponential curves. Then, the values of  $K_s$  obtained by each method were compared.

The results show that the values of  $K_s$  obtained using Method 2 were always between the values obtained using Method 1 and Method 3. Moreover, the dependence of Method 2 for the dynamic input parameters was less than the other two methods. Furthermore, it delivered the best coefficient of determination compared to the other two methods. Hence, Method 2 is proposed for calculating  $K_s$  while Method 1 and Method 2 can be utilized for the determination of the upper and lower bounds of  $K_s$ , respectively.

In this study, the minimum and maximum  $K_s$  was calculated as 14.8 GPa and 21.1 GPa for the hydrostatic stress values of 3.5 MPa and 24 MPa, respectively. As already mentioned, the value of matrix bulk modulus depends on the different minerals of each sample. For sandstone rocks, different values of  $K_s$  were reported by several researchers. For instance, Wang [21] measured the following values of  $K_s$  for different sandstone formations in the USA: Berea sandstone with 28.9 GPa, Ohio sandstone with 31 GPa, Weber sandstone with 36 GPa, Pecos sandstone with 39 GPa and Boise sandstone with 42 GPa. Furthermore, Hart and Wang [20] reported that the  $K_s$  values of Berea sandstone fluctuated from 25 to 34 GPa.

Moreover, the Skempton's coefficient of the sandstone samples relatively remained equal to 1 when the hydrostatic stress was kept less than 24.5 MPa, which is roughly equal to 50% of the wet samples' UCS. Thus, it was inferred that for a specific in situ hydrostatic stress less than 24.5 MPa, the Skempton's coefficient can be reasonably presumed equal to 1. Due to this, the laboratory experiments were conducted with a hydrostatic stress no larger than 24.5 MPa to avoid any failure within the samples' structures.

During the undrained tests, it was observed that, for the lower values of hydrostatic stress, the main proportion of the applied stress was borne by the pore water. The water withstood the applied hydrostatic stress released from the pore structures. However, as the hydrostatic stress increased, the role of the water bearing the applied pressure declined and, consequently, the matrix underwent larger stresses. Many researchers have already expressed that the active hydrostatic stress is one of the most influential parameters on the fluid motion (and fluid volume change) within the rock pores [26–30]. Moreover, the pore fluids soften the weak minerals surrounding the main matrix minerals, e.g., quartz, in sandstone rocks. This reduces the strength characteristics of the rock [31].

From the perspective of the rock failure criteria, the fluid pore pressure reduces the effective stresses acting on the rock matrix. This shifts the Mohr circle towards the left side (coordinate origin). Thus, the strength properties of the rocks, e.g., the bulk modulus, decrease due to the water presence and, consequently, the rock failure occurs at the lower magnitudes of shear stress.

The matrix bulk modulus is a key poroelastic parameter for understanding the rock response under the different loading conditions. The experimental procedure introduced in this research is an efficient way to calculate the poroelastic parameters of porous rocks. The obtained results also corroborate the findings achieved by [32,33], in which the matrix bulk modulus increased with the confining stress. The obtained results here can be used for studying the engineering phenomena related to the coupling between the pore fluid (water, oil, CO<sub>2</sub>, etc.) and the rock's solid matrix. Those potential phenomena are related to the possible applications in hydrogeology, civil engineering, mining engineering and geology engineering [34,35]. Moreover, the procedure presented here can be applied for the determination of the extraterrestrial poroelastic parameters through the acoustic wave propagation (seismic surveys) techniques on remote planets [36–38].

As the AVS apparatus works at a high frequency, the values of the undrained bulk modulus may be measured higher than the expected static values. This may result in an underestimation of the  $K_s$  values. To avoid this miscalculation, for future works, the  $K_s$  of the sandstone samples can be measured through static tests. The results of such static experiments can be compared to the results from those three methods applied in the current research. In this case, a better comprehension about the accuracy of each method is acquired. Furthermore, to evaluate the effects of the different parameters, i.e.,  $K$ ,  $K_u$ ,  $K_{dry}$ ,  $B$ ,  $\varphi$  and  $K_f$  on  $K_s$ , it is recommended to use creative mathematical algorithms such as the Monte Carlo simulation [39,40]. Applying such simulations helps to determine how the  $K_s$  varies with the different contributing factors.

## 5. Conclusions

In this research, three experimental methods were performed to measure the dynamic matrix bulk modulus of sandstone samples taken from the Świętokrzyskie Mine in Kielce, Poland. The results showed that, for a specific hydrostatic stress, the  $K_s$  values calculated using Method 2 were between the  $K_s$  values obtained using Method 1 and Method 3. The empirical correlation pertinent to Method 2 was extracted as follows

$$K_s = 15.251 P_C^{0.0097}$$

where  $K_s$  indicates the matrix bulk modulus (GPa) and  $P_C$  is the hydrostatic stress (MPa). For this correlation, the coefficient of determination was acquired as 0.70, thereby indicating a good fitness between the calculated values of  $K_s$  and the applied  $P_C$ . Furthermore, the minimum and maximum values of  $K_s$  were obtained as 14.8 GPa and 21.1 GPa for the hydrostatic stress values of 3.5 MPa and 24 MPa, respectively. Based on the extracted correlation, as the hydrostatic stress increased, the dynamic bulk modulus of the rock samples escalated exponentially.

It was also found that Skempton's coefficient fluctuated between 0.96 and 1 when the hydrostatic stress was less than 24.5 MPa. Hence, it can be said that the Skempton's coefficient can be considered as 1 when the hydrostatic stress is relatively equal to 50% of the wet samples' UCS (47.8 MPa).

The applied methodology can be used for the determination of the matrix bulk modulus in geoenvironmental projects in which the poroelastic response of the rock is of paramount importance. Some relevant projects include oil/gas extraction, EOR operation, hydraulic fracturing, waste disposal, land subsidence and aquifer engineering. As in natural reservoirs, when the rock is not under the dry conditions, the utilization of the dry bulk modulus in the calculations may give rise to the inaccurate estimation of the matrix bulk modulus. Thus, it is recommended that, for measurement of the matrix bulk modulus, the dry bulk modulus is not incorporated in the calculations.

**Author Contributions:** Conceptualization, D.K.; Methodology, D.K.; Software, M.K.; Validation, D.K. and M.A.M.Z.; Formal analysis, D.K. and M.K.; Investigation, M.K.; Resources, D.K.; Data curation, M.K. and M.A.M.Z.; Writing—original draft, D.K., M.K. and M.A.M.Z.; Writing—review & editing, D.K., M.K. and M.A.M.Z.; Visualization, D.K. and M.A.M.Z.; Supervision, D.K.; Project

administration, D.K.; Funding acquisition, D.K. All authors have read and agreed to the published version of the manuscript.

**Funding:** The project was supported by the AGH University of Science and Technology, Krakow, Poland, subsidy 16.16.190.779.

**Institutional Review Board Statement:** Not applicable.

**Informed Consent Statement:** Not applicable.

**Data Availability Statement:** All used data are accessible in the context of the article.

**Conflicts of Interest:** All authors of this paper declare no conflict of interest.

## References

1. Alyafei, N. *Fundamentals of Reservoir Rock Properties*, 2nd ed.; Hamad Bin Khalifa University Press: Doha, Qatar, 2021; ISBN 9789927137273. [\[CrossRef\]](#)
2. Fjaer, E.; Holt, R.M.; Horsrud, P.; Raaen, A.M.; Risnes, R. *Petroleum Related Rock Mechanics*, 2nd ed.; Elsevier: Amsterdam, The Netherlands, 2008; ISBN 978-0-444-50260-5.
3. Terzaghi, K.; Peck, R.B.; Mesri, G. *Soil Mechanics in Engineering Practice*, 3rd ed.; John Wiley & Sons: Hoboken, NJ, USA, 1996; ISBN 978-0-444-50260-5.
4. Biot, M.A. General Theory of three-dimensional consolidation. *J. Appl. Phys.* **1941**, *12*, 155–164. [\[CrossRef\]](#)
5. Wang, C.; Zeng, Z. Overview of Geomechanical Properties of Bakken Formation in Williston Basin, North Dakota. In Proceedings of the 45th U.S. Rock Mechanics/Geomechanics Symposium, San Francisco, CA, USA, 26–29 June 2011; pp. 1–11.
6. Zhang, J.J. *Applied Petroleum Geomechanics*, 2nd ed.; Elsevier Inc.: Cambridge, MA, USA, 2019; ISBN 978-0-12-814814-3. [\[CrossRef\]](#)
7. Mavko, G.; Mukerji, T.; Dvorkin, J. *The Rock Physics Handbook: Tools for Seismic Analysis of Porous Media*; Cambridge University Press: Cambridge, UK, 2009. [\[CrossRef\]](#)
8. Vukuturi, V.S. The effect of liquids on the tensile strength of limestone. *Int. J. Rock Mech.* **1974**, *11*, 27–29. [\[CrossRef\]](#)
9. Peck, L. Stress corrosion and crack propagation in Sioux quartzite. *J. Geophys. Res. Solid Earth* **1983**, *88*, 5037–5046. [\[CrossRef\]](#)
10. Jaeger, J.C. The effect of absorption of water on the mechanical properties of sandstones. *J. Inst. Eng. Aust.* **1943**, *15*, 164–166.
11. Rabat, Á.; Cano, M.; Tomás, R. Effect of water saturation on strength and deformability of building calcarenite stones: Correlations with their physical properties. *Constr. Build. Mater.* **2020**, *232*, 117259. [\[CrossRef\]](#)
12. Rutter, E.H. The influence of interstitial water on the rheological behaviour of calcite rocks. *Tectonophysics* **1972**, *14*, 13–33. [\[CrossRef\]](#)
13. Paterson, M.S.; Wong, T.F. *Experimental Rock Deformation: The Brittle Field*; Springer: Berlin/Heidelberg, Germany, 2005. [\[CrossRef\]](#)
14. Qin, X.; Han, D.H.; Zhao, L. Measurement of Grain Bulk Modulus on Sandstone Samples from the Norwegian Continental Shelf. *J. Geophys. Res. Solid Earth* **2022**, *127*, e2022JB024550. [\[CrossRef\]](#)
15. Makhnenko, R.Y.; Labuz, J.F. Saturation of Porous Rock and Measurement of the *B* coefficient. In Proceedings of the 47th US Rock Mechanics/Geomechanics Symposium, San Francisco, CA, USA, 23–26 June 2013.
16. Tarokh, A.; Detournay, E.; Labuz, J. Direct measurement of the unjacketed pore modulus of porous solids. *R. Soc.* **2018**, *474*, 20180602. [\[CrossRef\]](#)
17. Knez, D.; Zamani, M.A.M. Empirical Formula for Dynamic Biot Coefficient of Sandstone Samples from South-West of Poland. *Energies* **2021**, *14*, 5514. [\[CrossRef\]](#)
18. Zamani, M.A.M.; Knez, D. A new mechanical-hydrodynamic safety factor index for sand production prediction. *Energies* **2021**, *14*, 3130. [\[CrossRef\]](#)
19. Cosenza, P.; Ghoreychi, M.; de Marsily, G.; Vasseur, G.; Violette, S. Theoretical prediction of poroelastic properties of argillaceous rocks from in situ specific storage coefficient. *Water Resour.* **2002**, *38*, 25-1–25-12. [\[CrossRef\]](#)
20. Hart, D.J.; Wang, H.F. Laboratory measurements of a complete set of poroelastic moduli for Berea Sandstone and Indiana Limestone. *J. Geophys. Res.* **1995**, *100*, 17741–17751. [\[CrossRef\]](#)
21. Wang, H.F. *Theory of Linear Poroelasticity with Applications to Geomechanics and Hydrogeology*; Princeton University Press: Oxford, UK, 2000.
22. Rajaoalison, H.; Knez, D.; Zlotkowski, A. Changes of Dynamic Mechanical Properties of Brine-Saturated Itebna Sandstone under Action of Temperature and Stress. *Przemysł Chem.* **2019**, *98*, 801–804.
23. Knez, D.; Rajaoalison, H. Discrepancy between Measured Dynamic Poroelastic Parameters and Predicted Values from Wyllie's Equation for Water-Saturated Itebna Sandstone. *Acta Geophys.* **2021**, *69*, 673–680. [\[CrossRef\]](#)
24. Knez, D.; Rajaoalison, H.; Nkunzi, D. Drilling Mud Influence on Sandstone Poroelastic Parameters. *J. Geotechnol. Energy* **2022**, *39*, 5–13. [\[CrossRef\]](#)
25. Knez, D.; Rajaoalison, H. Land Subsidence Assessment for Wind Turbine Location in the South-Western Part of Madagascar. *Energies* **2022**, *15*, 4878. [\[CrossRef\]](#)
26. Nowakowski, A. The Influence of Rate of Change in Confining and Pore Pressure on Values of the Modulus of Compressibility of the Rock Skeleton and Biot's Coefficient. *Energies* **2021**, *14*, 3056. [\[CrossRef\]](#)

27. Knez, D. Stress State Analysis in Aspect of Wellbore Drilling Direction. *J. Arch. Min. Sci.* **2014**, *59*, 71–76. [[CrossRef](#)]
28. Knez, D.; Calicki, A. Looking for a New Source of Natural Proppants in Poland. *J. Bull. Pol. Acad. Sci. Tech. Sci.* **2018**, *66*, 3–8. [[CrossRef](#)]
29. Knez, D.; Mazur, S. Simulation of Fracture Conductivity Changes due to Proppant Composition and Stress Cycles. *J. Pol. Miner. Eng. Soc.* **2019**, *2*, 231–234.
30. Knez, D.; Wiśniowski, R.; Owusu, W.A. Turning Filling Material into Proppant for Coalbed Methane in Poland-Crush Test Results. *Energies* **2019**, *12*, 1820. [[CrossRef](#)]
31. Zhang, D.; Pathegama Gamage, R.; Perera, M.S.A.; Zhang, C.; Wanniarachchi, W.A.M. Influence of water saturation on the mechanical behaviour of low-permeability reservoir rocks. *Energies* **2017**, *10*, 236. [[CrossRef](#)]
32. Brown, J.M.; Journaux, B. Local-basis-function equation of state for ice VII–X to 450 GPa at 300 K. *Minerals* **2020**, *10*, 92. [[CrossRef](#)]
33. Mavko, G.; Vanorio, T. The influence of pore fluids and frequency on apparent effective stress behavior of seismic velocities. *Geophysics* **2010**, *75*, 1–7. [[CrossRef](#)]
34. Khalilidermani, M.; Knez, D.; Zamani, M.A.M. Empirical Correlations between the Hydraulic Properties Obtained from the Geoelectrical Methods and Water Well Data of Arak Aquifer. *Energies* **2021**, *14*, 5415. [[CrossRef](#)]
35. Fan, Z.; Eichhubl, P.; Newell, P. Basement fault reactivation by fluid injection into sedimentary reservoirs: Poroelastic effects. *J. Geophys. Res. Solid Earth* **2019**, *124*, 7354–7369. [[CrossRef](#)]
36. Knez, D.; Zamani, M.A.M. A Review of the Geomechanics Aspects in Space Exploration. *Energies* **2021**, *14*, 7522. [[CrossRef](#)]
37. Knez, D.; Khalilidermani, M. A Review of Different Aspects of Off-Earth Drilling. *Energies* **2021**, *14*, 7351. [[CrossRef](#)]
38. Khalilidermani, M.; Knez, D. A Survey of Application of Mechanical Specific Energy in Petroleum and Space Drilling. *Energies* **2022**, *15*, 3162. [[CrossRef](#)]
39. Quosay, A.A.; Knez, D. Sensitivity Analysis on Fracturing Pressure Using Monte Carlo Simulation Technique. *Oil Gas Eur. Mag.* **2016**, *42*, 140–144.
40. Quosay, A.A.; Knez, D.; Ziaja, J. Hydraulic Fracturing: New Uncertainty Based Modeling Approach for Process Design Using Monte Carlo Simulation Technique. *PLoS ONE* **2020**, *15*, e0236726. [[CrossRef](#)] [[PubMed](#)]

**Disclaimer/Publisher’s Note:** The statements, opinions and data contained in all publications are solely those of the individual author(s) and contributor(s) and not of MDPI and/or the editor(s). MDPI and/or the editor(s) disclaim responsibility for any injury to people or property resulting from any ideas, methods, instructions or products referred to in the content.